

# Measurements of the Beam-Wave Fluctuations over a 142-km Atmospheric Path

N. Perlot, D. Giggenbach, H. Henniger, J. Horwath, M. Knappek and K. Zettl  
DLR, Institute of Communication and Navigation, 82234 Wessling, Germany

## ABSTRACT

An optical link has been established between the Canary Islands La Palma and Tenerife. A 1064-nm transmitting laser was located on La Palma whereas a BPSK communication receiver and measurement instruments were installed in ESA's OGS on Tenerife. Beside the demonstration of a high-data-rate coherent signal transmission, the goal of the experiment was to measure the effects of the atmosphere on the beam propagation in order to estimate its impact on optical links. Wavefront distortions have been investigated by means of a DIMM instrument and scintillation was observed by imaging the pupil of the OGS telescope on a CCD camera. Strong scintillation was observed during the entire campaign with scintillation peaks at sunsets and sunrises, and saturation at about noon. Because of the narrowness of the beam (10- $\mu$ rad divergence), beam wander has been a serious issue. Statistical results are compared with theory.

**Keywords:** Free-space optics, optical turbulence, wavefront distortions, scintillation

## 1. INTRODUCTION

In October 2005 an experiment has been performed to test the receiver part of the coherent homodyne BPSK laser communication terminal (LCT) built by TESAT Spacecom under atmospheric impacts. The background of this campaign is the in orbit verification of the LCT. The German TerraSAR-X LEO satellite mission with synthetic aperture radar as primary payload and the LCT as secondary payload will be launched at the end of 2006. In addition to the coherent signal detected by the BPSK receiver, data on the level of wavefront distortions and scintillation have been gathered. Meaningful measurements could be performed over 5 days.

## 2. SCENARIO DESCRIPTION

### 2.1 Geographical Situation

The link was established in the Canary Islands (see Fig. 1) between La Palma and Tenerife. The transmitter was on La Palma where a portable measurement container has been used. The location of the container has been selected according to environmental conditions. The criterion was an as high as possible sight to the OGS without fog. Therefore the Tx-container has been placed on the side of a road, several kilometers away from European Northern Observatory. It is generally known that, from this location, clouds stemming from the volcano crater "Caldera de Taburiente" do not cross the line of sight. On Tenerife, the receiver was located in the Optical Ground Station (OGS) of the European Space Agency (ESA). The link has been performed over a distance of  $L = 142$  km. The major part of the link was at an altitude of 2 km over the Atlantic Ocean. A height profile of the link can be seen in Fig. 2. A similar link was reported in 1990, the locations of transmitter and receiver were reversed though [1].

Unfortunately, the weather conditions during the trial period have not been as good as expected. Heavy fog blown from the Caldera towards the Tx-Container, suspended Sahara sand particles (Kalima), strong wind forbidding an opening of the OGS-dome, rain and other bad weather conditions decreased the measurement time.



Fig. 1 Geographical view of the 142-km link between the La-Palma and Tenerife islands

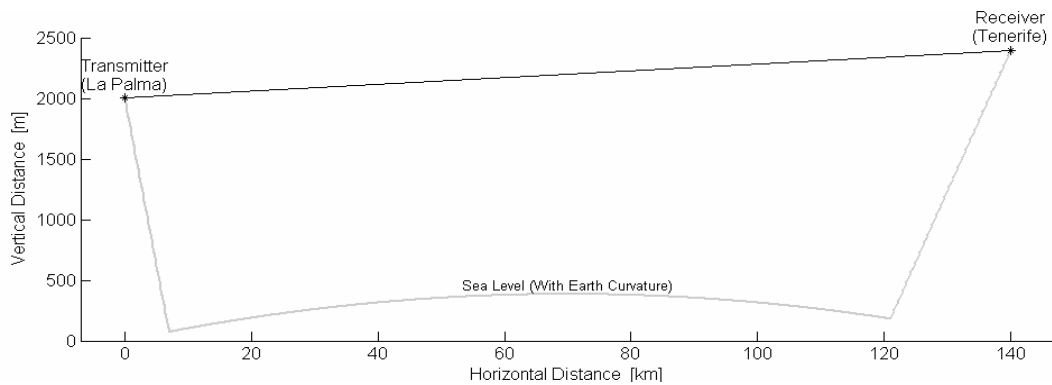


Fig. 2 Vertical cross section of the terrain over which the link has been performed.

## 2.2 Transmitter

The beam sent from the La Palma island was a single mode ( $TEM_{00}$ ) Gaussian beam with a wavelength  $\lambda = 1.064 \mu\text{m}$ . The beam was collimated with a half divergence angle of  $\theta_{div} \approx 10 \mu\text{rad}$  and a transmit radius of  $W_0 = \lambda / \pi \theta_{div} \approx 3.4 \text{ cm}$ . The corresponding Rayleigh range of the beam equals  $L_R = \lambda / \pi \theta_{div}^2 \approx 3.4 \text{ km}$ . The output power was 1.2 W.

## 2.3 Receiver

The telescope of the OGS is a 1-m cassegrain telescope. A part of the optical field received by the 1-m telescope was directed to the 65-mm aperture of the coherent receiver (see Fig. 3). The optical field over the LCT aperture was detected coherently (for communication) and incoherently (for measurement). Additionally the telescope pupil was imaged on a CCD camera and supapertures of the telescope pupil were used for the DIMM instrument.

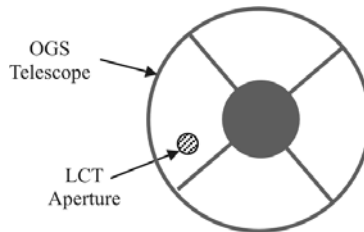


Fig. 3 View of the LCT aperture within the 1-m telescope aperture.

### 3. RESULTS OF THE COHERENT COMMUNICATION

The results of the communication link have been published in a previous paper [2]. A 5.6-Gbit/s BPSK signal could be transmitted.

### 4. WAVEFRONT FLUCTUATIONS

#### 4.1 The DIMM Instrument

The Differential Image Motion Monitor (DIMM) enables the estimation of the Fried parameter  $r_0$  which characterizes the atmospheric wavefront distortions [3]. Two subapertures are created in the telescope pupil with a given separation between the subapertures.

#### 4.2 Results

The  $r_0$  values estimated by the DIMM instrument are shown in Fig. 4. A good  $r_0$  parameter (larger than 15 cm) was recorded on the 4<sup>th</sup> of October. For other days where measurements could be performed,  $r_0$  was much smaller. The  $r_0$  values measured in the night were larger than in the day.

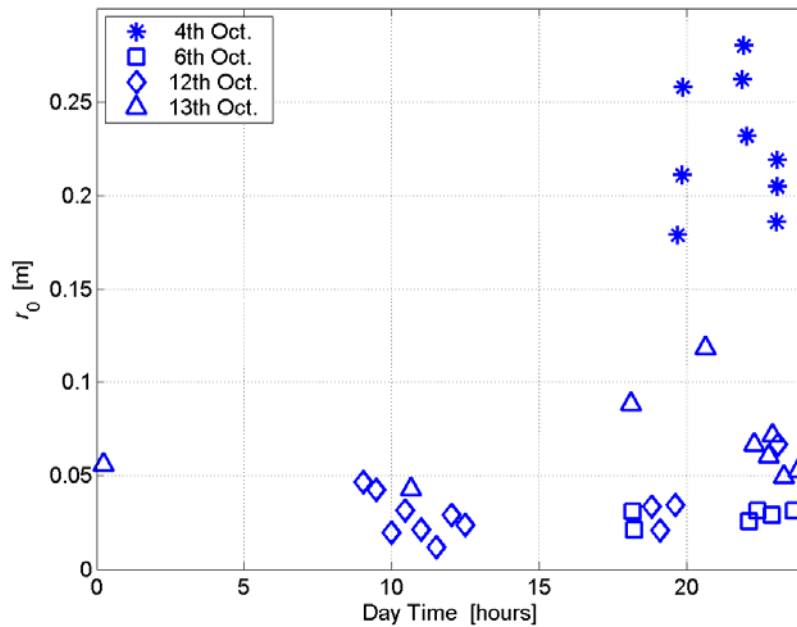


Fig. 4 Fried Parameter  $r_0$  over the day measured by a DIMM instrument.

### 5. SCINTILLATION

#### 5.1 Pupil Measurements

Images of the telescope pupil have been recorded. Fig. 5 shows typical scintillation speckles on the pupil of the OGS telescope at different times of the day. From the recorded pupil images, the intensity correlation estimated was estimated according to two different definitions: as either the  $1/e$  or the  $1/e^2$  crossing point of the covariance function. Results are gathered in. Fig. 6 where the darkness of the markers encodes the definition used for the correlation length.

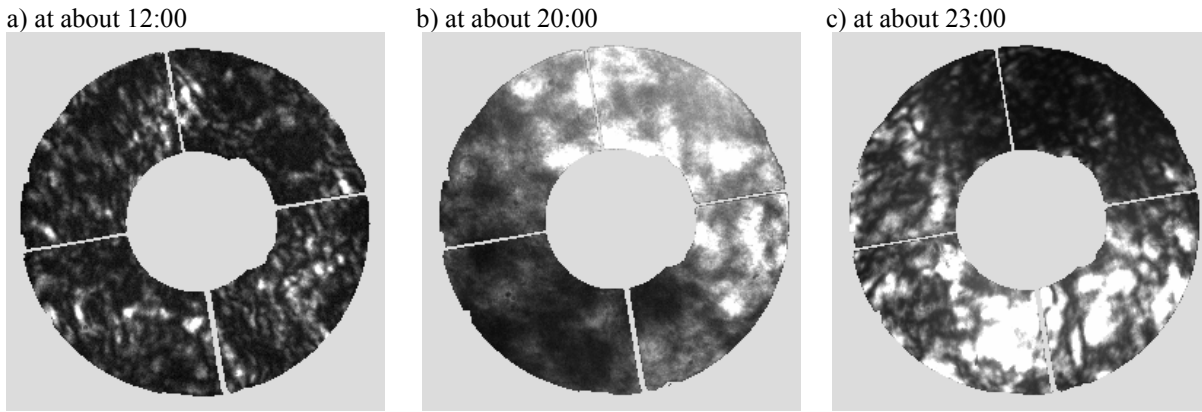


Fig. 5 typical pupil images of OGS receiver telescope (1-m diameter).

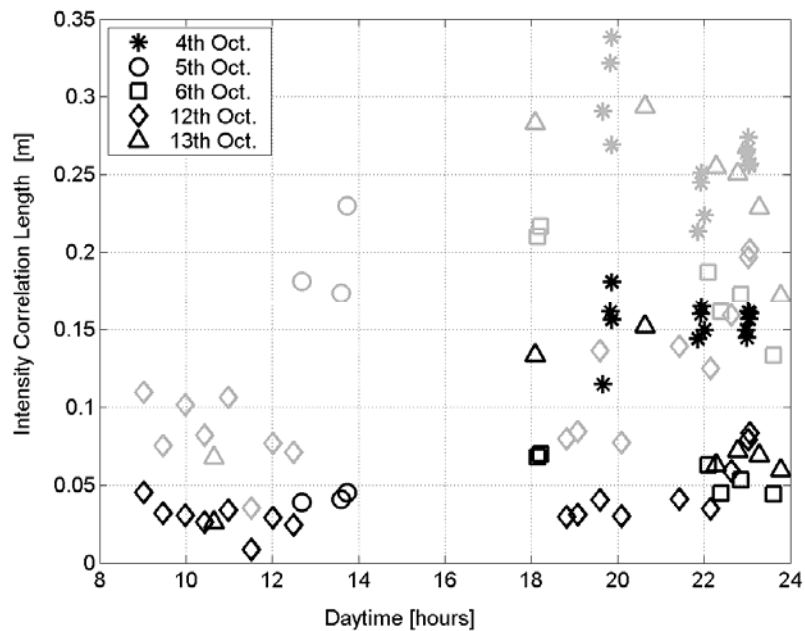


Fig. 6. Intensity correlation length (mean speckle size) evaluated from the recorded telescope pupils. Two types of correlation length have been considered: the dark markers denote the  $1/e$  crossing point whereas the bright markers denote the  $1/e^2$  crossing point of the covariance function.

Comparing those data with the predictions of scintillation theory, we can draw several conclusions.

- The maximum theoretical correlation length (defined as the  $1/e$ -crossing point) is about 38 cm as given by the formula  $1.2\sqrt{\lambda L}$  valid for a spherical wave in the weak-fluctuation regime [4]. Since all measured correlation lengths are clearly under this value, the link lies in any case in the strong-fluctuation regime.
- Around noon, the correlation length takes its lowest values (around 2 cm). Turbulence is strong causing the scintillation to saturate.
- In the evening and in the night, the correlation length becomes larger: turbulence is weaker and scintillation lies close to the focusing regime.

## 5.2 Estimation of the Rytov Index and the $C_n^2$

In this inter-island scenario, scintillation was found to vary between the so-called focusing regime where turbulence is weak but the scintillation index is maximum, and the saturation regime where turbulence is strong.

Using the Rytov index  $\sigma_R^2$  as a measure of the scintillation level, we estimate that  $\sigma_R^2$  varied approximately between 5 and 500 during the trial period. From the definition of the Rytov index  $\sigma_R^2$ , we can also estimate the  $C_n^2$  which is then given by [5]

$$C_n^2 = \frac{\sigma_R^2}{1.23k^{7/6}L^{11/6}} \quad (1)$$

$C_n^2$  is here assumed constant. The  $C_n^2$  range is given in Table 1. Additionally, the corresponding theoretical  $r_0$  for the transmitted Gaussian beam described in Section 2.2 is given [4]. This  $r_0$  is very close to that of a spherical wave.

	Min	Max
$\sigma_R^2$	5	500
$C_n^2$ [ $\text{m}^{-2/3}$ ]	$1.8 \times 10^{-17}$	$1.8 \times 10^{-15}$
$r_0$ [m]	0.20	0.013

Table 1 Estimated range of the turbulence parameters during the trial

## 5.3 Optical Power Collected by a 65-mm Aperture

The optical power over the 65-mm terminal aperture was received on a PIN diode and sampled at a rate of 1 kHz. The power scintillation index was estimated on a 1-minute interval and plotted in Fig. 7 over the day time. Fig. 7 represents data gathered over three days. Scintillation indices less than one can be observed when scintillation was highly saturated and thus significant aperture averaging occurred. This was mostly observed in the middle of the day when turbulence is the strongest, but it also occurred around 20:00. What is remarkable is the high variation of the scintillation index during some periods that mostly occurred in the evening and in the night. Values have for example varied between 4 and 9 over only several minutes. It is believed that during those periods a strong beam wander appeared due to turbulence above the ground near the transmitter. These beam deviations would then be slow enough to create variations of the scintillation statistics from one minute to another. Indeed, the mean power was found to vary significantly between one and the next minute.

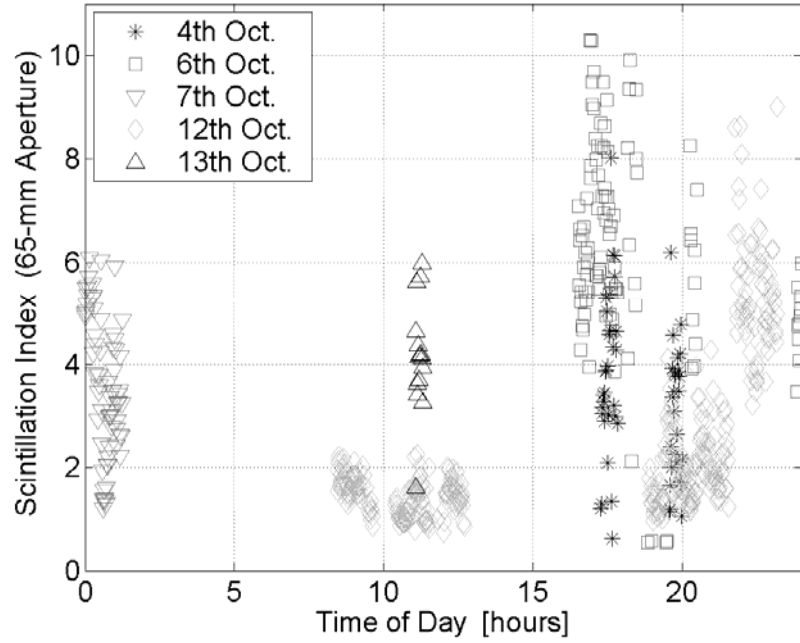


Fig. 7. Overview of normalised power Variance (power scintillation index) during the Trial (data of three days have been merged here).

One particular minute of received power has been considered and the estimated probability density function (PDF) and power spectral density (PSD) are shown in Fig. 8 and Fig. 9 respectively. Most variations of the received power were found to be contained in the band 0 - 100 Hz.

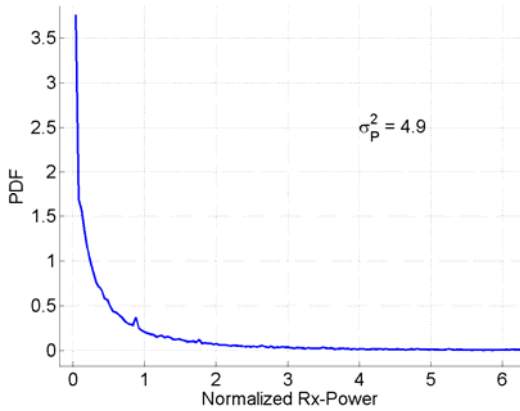


Fig. 8. PDF of the normalized power collected by the 65-mm aperture. Data over 1 minute are considered. The scintillation index was estimated at  $\sigma_p^2 = 4.9$ .

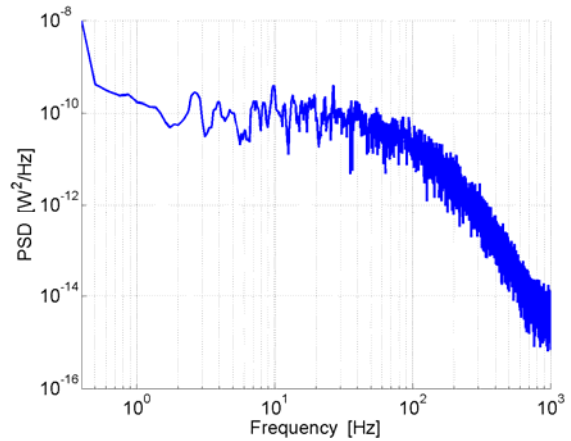


Fig. 9. Power spectral density of the optical power collected by the 65-mm aperture.

#### 5.4 Scintillation Theory

Having a strong-fluctuation scenario, we evaluated numerically the scintillation index using the modified Rytov for a Gaussian beam [5]. Transmitter beam parameters of Section 2.2 have been used as well as a constant  $C_n^2$  ranging

between the values of Table 1. Even for a point receiver and a high inner scale ( $l_0 = 1$  cm), the predicted scintillation index is around 3 and remains less than some values shown in Fig. 7.

## 5.5 Beam Wander

With an infrared viewer, we could observe during the night the wander of the beam spot on the walls of the OGS. Beam-centroid deviations of more than 1 meter were regularly observed. To theoretically study the scintillation induced by beam wander, we consider the parameter  $\beta$  which is the ratio of the root-mean-square displacement  $\sqrt{\langle r_c^2 \rangle}$  of the short-term beam spot to its radius  $W_{ST}$ :

$$\beta = \frac{\sqrt{\langle r_c^2 \rangle}}{W_{ST}} \quad (2)$$

The rms displacement is given by ([4] in Section 6.5.4)

$$\langle r_c^2 \rangle = 2.87 C_n^2 L^3 W_0^{-1/3} \quad (3)$$

where  $W_0$  is the radius of the collimated beam at the transmitter. Because Eq. (3) is based on phase-front statistics, its validity can be reasonably prolonged to the strong-fluctuation regime [6].

The short-term beam radius can be evaluated from ([4] in Section 12.2.3)

$$\begin{aligned} W_{ST}^2 &= W_e^2 - \langle r_c^2 \rangle \\ &= W^2 \left( 1 + 1.625 (\sigma_R^2)^{6/5} \Lambda - 2.87 C_n^2 L^3 W_0^{-1/3} \right) \end{aligned} \quad (4)$$

where  $\sigma_R^2$  is defined by Eq. (1) and

$$\Lambda = \frac{2L}{kW^2}. \quad (5)$$

Assuming a beta distribution for the fluctuations due to beam wander [7], the component  $\sigma_{BW}^2$  of the scintillation index due solely to beam wander is

$$\sigma_{BW}^2 = \frac{(1 + \beta^2)^2}{1 + 2\beta^2} - 1. \quad (6)$$

With the following parameters:  $W_0 = 3.4$  cm,  $\lambda = 1064$  nm,  $L = 142$  km,  $W = 1.4$  m, we obtain the results of Fig. 10. The  $\beta$  value obtained for  $C_n^2 = 1.8 \times 10^{-16} \text{ m}^{-2/3}$  is close the maximum values allowed by Eqs. (2) to (4). To obtain the total irradiance fluctuations, the beam-wander fluctuations must be modulated by the scintillation present "within" the beam. However, even with this modulation, the values of  $\sigma_{BW}^2$  are certainly not high enough to explain the high scintillation indices observed in Fig. 7. One explanation is that the assumption of a  $C_n^2$  profile is not valid: turbulence above the ground near the transmitter is significantly stronger than for the rest of path. This would result in a stronger beam wander.

$C_n^2$ [ $\text{m}^{-2/3}$ ]	$1.8 \times 10^{-17}$	$1.8 \times 10^{-16}$	$1.8 \times 10^{-15}$
$\beta$	0.47	0.88	0.71
$\sigma_{BW}^2$	0.034	0.24	0.13

Fig. 10 Theoretical beam wander parameters

## 6. ATMOSPHERIC EFFECTS ON COHERENT SIGNAL

### 6.1 Coherent-System Evaluation Graph

In order to identify the sources of receiver performance degradation, received signal samples have been plotted in a two dimensional plot which we call a coherent-system evaluation graph (CSEG). In this graph, the amplitude of the coherent signal is plotted as a function of the amplitude of the incoherent signal. Thus, such a plot in experimental conditions is possible only when the coherent signal and the collected power are measured simultaneously. The photocurrent  $i_{coh}$  bearing the coherent signal is proportional to:

$$i_{coh} \propto \sqrt{\eta_{het} P_{Rx}}, \quad 0 \leq \eta_{het} \leq 1 \quad (7)$$

where  $\eta_{het}$  is the instantaneous heterodyne efficiency and  $P_{Rx}$  is the received optical power. The heterodyne efficiency is related to  $r_0$  and measures the goodness of the superposition of the local oscillator on the received field (see for example [8]). The photocurrent  $i_{incoh}$  of a direct-detection receiver is proportional to the received optical power:

$$i_{incoh} \propto P_{Rx} \quad (8)$$

In the CSEG, we plot  $\eta_{het} P_{Rx}$  with respect to  $P_{Rx}$  with logarithmic scales as shown in Fig. 11. Since the heterodyne efficiency is less than 1, measured sample points appear only in the lower right part of the CSEG. Without atmospheric disturbances, all received signal samples are constant and correspond to a single point in the graph which is the intersection of the lines  $y = x$  and  $x = \langle P_{Rx} \rangle$ .

Fading in the coherent signal is counted when  $\eta_{het} P_{Rx}$  goes under a minimum level which is given by the communication requirements. This minimum signal is represented by the horizontal dotted line in Fig. 11. Fades are categorised in three different types:

- scintillation fades
- wavefront fades
- wavefront and scintillation fades (both combined)

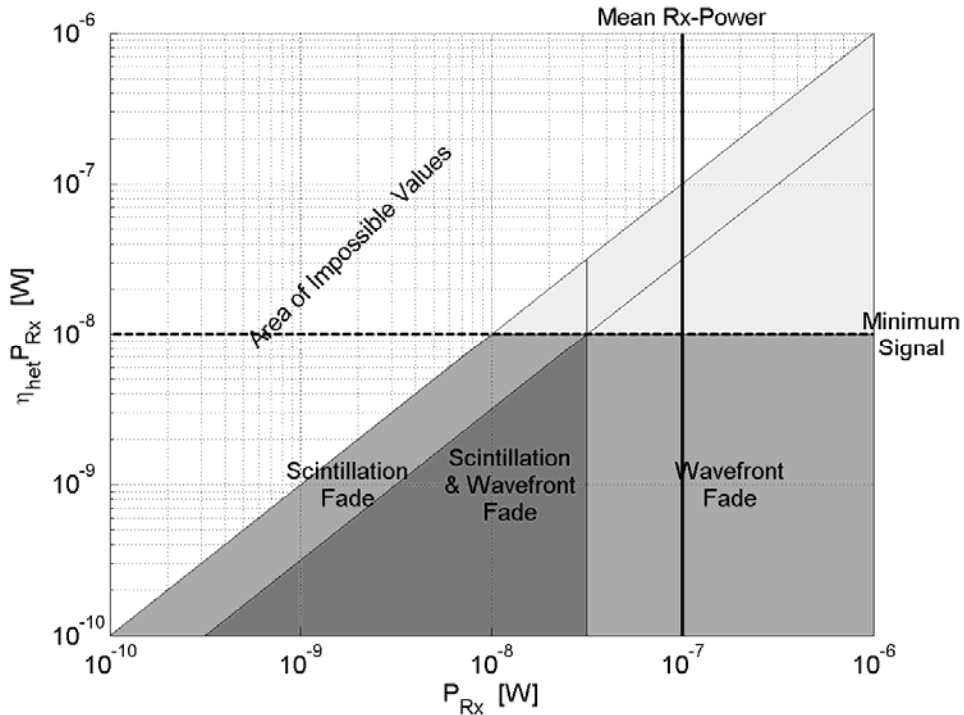


Fig. 11 Graph used to evaluate the coherent system and the sources of signal fading.



## 6.2 Experimental Results

The optical field received on Tenerife was split in order to enter both the coherent communication terminal and a direct detector. Both receivers had an aperture diameter of 65 mm. The direct detector consisted of an InGaAs PIN diode. From the communication terminal, the coherent signal  $i_{coh}$  was measured and the corresponding equivalent optical power  $\eta_{het} P_{Rx}$  could be retrieved using the curve  $i_{coh} = f(\eta_{het} P_{Rx})$  that was previously measured in the laboratory. We then plotted each doublet  $(P_{Rx}, \eta_{het} P_{Rx})$  of a given period in the CSEG. Typical data observed over 1 minute are shown in Fig. 12. Here we defined the minimum coherent signal as the signal giving a BER of  $5 \times 10^{-3}$ . This represents an equivalent power of  $\eta_{het} P_{Rx} = 10^{-8}$  W (-50 dBm). Fading statistics are shown in the upper left part of the graph. The signal was too low 20.8 % of the time and wavefront distortions have caused alone 7 % of the fades. Note that low signal values were sampled at a low resolution. This creates an alignment of low powers and equivalent powers at some particular levels, and misleads the interpretation of the graph in terms of point density.

Wavefront distortions and scintillation have caused the coherent signal to fluctuate over several orders of magnitude. These highly fluctuating values have led to highly fluctuating BERs as reported in [2].

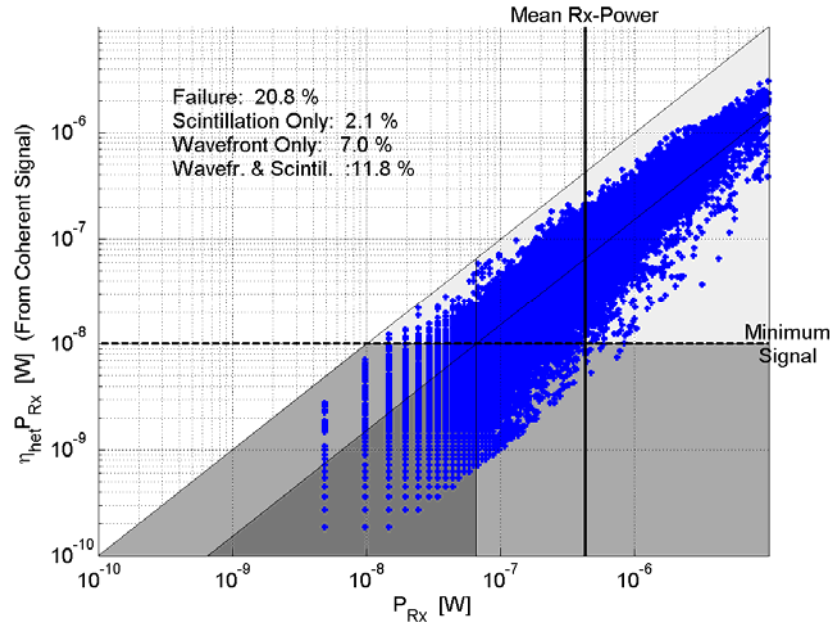


Fig. 12 Typical CSEG obtained during the 142-km inter-island link. 60000 samples obtained over 1 minute have been plotted.

## 7. CONCLUSIONS

During the trial period, the dynamic of atmospheric turbulence conditions was very large. The state of the atmosphere often changed within a short time. However, some trends could be observed in particular for scintillation. The Fried parameter  $r_0$  has been measured between 1.2 cm and 28 cm. Most of the time,  $r_0$  was slightly smaller than the Rx-aperture size (6.5cm).

The mean received power over the whole trial period varied over several orders of magnitude. Also the short-term dynamic of the received power was around 40 dB. On the one hand, a collimated beam from the transmitter avoided a too weak mean signal power at the receiver. On the other hand, with a collimated beam, the scintillation rose dramatically due to beam wander caused by turbulence at the transmitter, deflecting the complete beam. Very high scintillation indices of up to 10 were observed for a 6.5-cm aperture.

The size of the  $r_0$  parameter and the size of intensity speckles with respect to the LCT aperture varied strongly during the day. In general, the size of terminal aperture (6.5 cm) was well dimensioned for the encountered average  $r_0$ .

## 8. REFERENCES

- [1] A. Comeron et al: "Inter-Island Optical Link Tests", IEEE Photonics Technology Letters, Vol. 2 No. 5, May 1990
- [2] R. Lange, B. Smutny, B. Wandernoth, R. Czichy and D. Giggenbach, "142 km, 5.625 Gbps Free - Space Optical Link based on homodyne BPSK modulation", *Proc. Of SPIE, Free-Space Laser Communication Technologies XVIII*, V. 6105, 2006.
- [3] M. Sarazin, F. Roddier, "The ESO differential image motion monitor", *Astronomy & Astrophysics*, 227, 294-300, 1990.
- [4] L. C. Andrews, R. L. Phillips, *Laser Beam Propagation through Random Media*, SPIE Press, Bellingham, 1998
- [5] L. C. Andrews, R. L. Phillips, C. Y. Hopen, *Laser Beam Scintillation with Applications*, SPIE Press, Bellingham (WA), USA, 2001.
- [6] V. I. Tatarski, *Wave propagation in a turbulent medium*, McGraw-Hill, New York, 1961
- [7] K. Kiasaleh, "On the probability density function of signal intensity in free-space optical communications systems impaired by pointing jitter and turbulence," *Opt. Eng.*, vol. 33, no. 11, pp. 3748–3757, 1994.
- [8] S. C. Cohen, "Heterodyne detection: phase front alignment, beam spot size, and detector uniformity," *Appl. Opt.* **14**, 1953-1959; 1975: